Visualizing the Brain Structure with a DT-MRI Minimum Spanning Tree

Prompong Pakawanwong

Graduate School of Information Science and Technology,
The University of Tokyo, Japan
prompong@is.s.u-tokyo.ac.jp

Abstract. Visualizing the human brain using diffusion tensor magnetic resonance imaging (DT-MRI) data has been a key technique to study the structure of the human brain and its connectivity. The challenge is to find a method that best exploits the data and serves as a model for visualization and connectivity analysis. This paper presents a novel method of visualizing the human brain structure with a minimum spanning tree using DT-MRI data. The human brain is modeled as a graph in which each vertex represents a brain voxel and each edge represents connectivity between a pair of neighboring brain voxels, resulting in each vertex having 26 weighted connections with adjacent voxels. The weight of an edge is calculated from the DT-MRI data with a higher weight assigned to an edge that are more likely aligned with nerve fiber trajectories. The method then grows a minimum spanning tree representing paths of the nerve fiber bundles. The resultant minimum spanning tree is consistent with the known anatomical appearances of the human brain. As the minimum spanning tree representing the human brain is a global deterministic model with well-defined connectivity between voxels in the brain, it can serve not only as a deterministic visualization of the human brain but also as an instrument for connectivity analysis. In addition, this method overcomes several problems present in previous methods such as tracking termination in traditional fiber tracking and meaningless streamlines in stochastic connectivity mapping.

Keywords: Diffusion tensor magnetic resonance imaging, brain visualization, minimum spanning tree

1 Introduction

The human brain, the center of the human nervous system, is a complex organ. In a volume less than 1.5 liters lie billions of nerve cells constituting an extremely complicated network [1, 11, 15, 20, 26, 12, 41–43, 18]. Myelinated nerve fibers, connecting parts of the human brain, extend to the length of more than one hundred thousand kilometers [29, 44]. Although it has been known for a long time that the human brain was the center of the human nervous system, it was not possible to study the human brain in vivo (in a living person) until the arrival of recent medical imaging technologies such as radiography and computed tomography [33, 34]. However, the clinical technique considered to be the breakthrough in human brain visualization is diffusion tensor magnetic resonance imaging (DT-MRI), the first non-invasive in vivo imaging technique

that measures water diffusion in living tissues [27]. Exploiting the fact that water diffusion has different characteristics in different types of brain tissues, DT-MRI allows differentiating between different areas of the human brain and visualizing them [5, 6, 38]. It has constantly been proven to be an effective technique. Several neurological disorders such as multiple sclerosis, stroke, and trauma are characterized by changes in brain tissues or connections, which can be diagnosed by DT-MRI [14, 32, 48, 49, 47, 51]. In addition, connectivity analysis based on DT-MRI data reveals correlation between anatomical characteristics of the human brain and quantities such as intelligence quotient [16, 17, 28].

As DT-MRI provides raw information on water diffusion at centers of voxels on the three-dimensional human brain grid, one way to visualize the DT-MRI dataset is vector field visualization. Glyphs, graphical icons, can be used to represent diffusion tensors [19, 23, 24, 37]. In order to convey diffusion information, glyphs are parameterized by diffusion quantities computed from the diffusion tensors they represent such as mean diffusivity, dominant direction of diffusion, and anisotropy. While glyph-based techniques are capable of visualizing the underlying information of the human brain, they have some certain limitations. Glyphs on the three-dimensional grid can be too visually dense. Visual occlusion may prevent the grids from conveying information. More importantly, glyphs primarily show the local information of the individual voxels. The structure of the human brain, on the contrary, is characterized by connections between parts of the brain. That means, while diffusion glyph visualization techniques allow us to explore the diffusion activities in the human brain, they are not a precise tool for visualizing the human brain structure.

Since the beginning of the twenty-first century, the dominant method for visualizing the human brain structure utilizing DT-MRI data has been fiber tracking [8, 13, 30, 39, 45]. The term fiber tracking generally refers to a collection of methods that exploit the DT-MRI data to reconstruct the fiber tracts in the human brain. Based on the neuroanatomical fact that water diffuses faster along the myelinated fiber tracts, fiber tracking follows the dominant eigenvector of the diffusion tensor field in the DT-MRI dataset to generate curves representing the fiber tracts. The curves are then visualized to show the structure of the human brain. The explained fiber tracking algorithm, commonly referred to as traditional fiber tracking, is a forward leap in human brain visualization as it reveals information on structures and connectivity of the human brain. Nevertheless, traditional fiber tracking suffer from some problems. To begin with, traditional fiber tracking is not tolerant of noise and errors. DT-MRI data are normally discrete, coarsely-sampled, noisy, and voxel-averaged. Consequently, the dominant eigenvector, the eigenvector that the fiber tracking algorithm assumes to represent the fiber trajectories, may be incorrectly rendered. Following only the dominant eigenvector may result in errors or false fiber tract trajectories. In addition, traditional fiber tracking typically grows fibers iteratively. In each iteration, the algorithm adds to the end of an existing polyline a short line segment, the direction of which is determined by values locally calculated from the DT-MRI data. Thousands of iterations are usually performed to draw one polyline representing a fiber tract trajectory. Although the noise and errors are arguably negligible, the nature of traditional fiber tracking results in accumulation of those noise and errors to a significant amount, which may considerably set the fiber

tract trajectories off course. Second, traditional fiber tracking neglects the nature of fiber tract trajectories that fiber tracts neither are uniformly distributed nor behave like an orderly collection of curves; at some points fiber tracts cross, kiss, branch, or merge. Traditional fiber tracking is not capable of completely reconstructing fiber tracts with such characteristics. In addition, while studying the structure of the human brain aims at exploring its connectivity, traditional fiber tracking provides only implied connections as its output is simply a set of polylines drawn in three-dimensional space. One may imply that two regions of the human brain are interconnected if, for instance, there exists a polyline whose two endpoints are in the regions. Implying connections and connectivity analysis become more difficult if the resultant fiber tracts appear to be torn or rough.

The other notable method for visualizing the human brain structure using DT-MRI data is connectivity mapping [10, 25, 35, 36]. Unlike traditional fiber tracking, which follows the dominant eigenvector in the DT-MRI data to generate fiber tracts, connectivity mapping iteratively generates random paths using a probabilistic model such as Bayesian formulation from a given seeding voxel. After a number of iterations, the probability that the seeding voxel and any other voxel of interest are connected is equal to the number of random paths passing through that voxel divided by the number of random paths generated. Even though this method gives brain connectivity information, it has some drawbacks. First, the fiber tract trajectories in the human brain are not reconstructed; the output of this method is the probability values that pairs of voxels are connected. Even though the visualizations somehow resemble the fiber tracts, they should not be interpreted as such due to the fact that the trajectories are not well-defined. Second, the method is probabilistic, which means that it does not always produce the same results. It requires a certain amount of iterations in order to justify the results, which make the method a computational workload.

In this paper, we propose a deterministic method of visualizing the human brain structure with a minimum spanning tree utilizing DT-MRI data. Our method offers a concretely-defined model that conforms with the nature of the human brain, provides ascertained brain connectivity, and mitigates the problem of local noise and errors. In terms of visualization, our method provides a brain connectivity map that displays the fiber structures and can serve as a tool for connectivity analysis.

2 Methodology

In this chapter, we explain our method and its rationality.

2.1 Problem formulation

Given the nature of the human brain that it is a network that has evolved to have adequate connections, we propose that an equivalent formulation of reconstructing the fiber tract structures in the human brain in terms of graph theory is finding a minimum spanning tree in a given undirected weighted graph.

2.2 Human brain modeling

The human brain is modeled as an undirected weighted graph. Each brain voxel in a three-dimensional DT-MRI grid is mapped to a vertex of the graph. Each edge of the graph connects a pair of vertices that represent a pair of neighboring voxels. Each voxel not at the boundary has 26 neighboring voxels as a consequence. This results in a graph representing the human brain. Then, the weight is calculated and assigned to the edges in the manner that the lower weight represents higher likeliness that two voxels are connected by fiber tract. The definition of the weight is explained in the next section.

2.3 Defining weight of the edges

The weight of the edges implies the likeliness that the two neighboring voxels are connected by fiber tract. The more likely the two neighboring voxels are connected, the less the weight of the edge. The following weight calculation formula is based on the neurological assumption that fiber tracts are smooth and do not make sharp turns [21]. In the similar manner, fiber tracking algorithms are aborted when the fiber tracts have high curvature [8, 22, 31]. The following paragraphs discuss the measures that are taken into account when calculating the weight of the edges.

Figure 1 shows the situation where a fiber tract passes through two neighboring voxels of interest. Each square represents a brain voxel and each arrow represents an eigenvector. Based on the neurological assumption that fiber tracts are smooth and do not make sharp turns, the vector difference of the eigenvector of the first voxel that closest aligns with the fiber tract trajectory and the eigenvector of the second voxel that closest aligns with the fiber tract trajectory is likely the smallest compared to other vector differences of any other eigenvector of other neighboring voxels of the voxels of interest through which the fiber tract does not pass and any other eigenvector of the voxels of interest. Therefore, we propose that the vector difference of eigenvectors of two neighboring voxels is a valid measure for calculating the weight of the edge.

However, the aforementioned vector difference alone is not sufficient to comprise the weight of the edges as the relative position of one voxel with respect to the other voxel must also be taken into account. Figure 2 and Figure 3 illustrate two situations where two selected eigenvectors have equal direction and magnitude but are positioned differently. In Figure 2, the selected eigenvector of the first voxel points directly to the center of the second voxel. This exhibits the case that it is most likely that two voxels are connected by fiber tract. In Figure 3, on the contrary, two selected eigenvectors are parallel. This exhibits the case that the fiber tracts passing through the two voxels, if any, are most like parallel and, consequently, the two voxels are most likely not connected. To incorporate the relative position of one voxel with respect to the other voxel into the weight of the edge connecting two voxels, we propose two other measures: 1) the vector difference of the selected eigenvector of the first voxel of interest and the normalized vector that has the same direction as the vector from the center of the first voxel of interest to the center of the second voxel of interest and 2) the vector difference of the selected eigenvector of the second voxel of interest and the normalized vector that has the same direction as the vector from the center of the first voxel of interest to the center of the second voxel of interest.

One problem with the eigenvectors from the DT-MRI dataset is that they point along only one direction of the fiber tract while, in fact, at any point on the fiber tract the fiber tract extends to both directions [7]. Therefore, the direction of the eigenvectors must be reversed if necessary to agree with the direction from the first voxel of interest to the second voxel of interest, or the vector differences will not faithfully reflect the likeliness of the connection between the two voxels. Figure 4 and Figure 5 illustrate the explained situation. To determine whether the sign of the eigenvectors must be reversed, the dot product of two vectors are calculated before calculating the vector difference. If the dot product is positive, which means the direction of the vectors agree with the direction from the first voxel of interest to the second voxel of interest, preserve the direction of the vectors. If the dot product is negative, the direction of one of the vectors is reversed before calculating the vector difference.

Having calculated all three measures, we propose that the weight of the edges equals the sum of the magnitudes of the three vector differences, as shown in Figure 6. By taking every voxel as the first voxel of interest and every of its neighboring voxels as the second voxel of interest, one can calculate the weight of all the edges and complete the construction of the undirected weighted graph representing the human brain.

2.4 Selecting the eigenvectors

In the previous section, we propose the formula for calculating the weight of the edges by using eigenvectors in each diffusion tensor. The question is, however, which eigenvector truly represents the fiber tract in the voxel? In other words, which eigenvector should be selected for calculating the weight of the edges? Several fiber tracking algorithms assume that only the dominant eigenvector of the diffusion tensor is parallel to and hence reflects the fiber tract alignment [8, 13, 30, 31, 39, 45]. Nevertheless, this assumption ignores two important facts. First, the fiber tract structure of the human brain is complicated. The fiber tracts neither are uniformly distributed nor behave like a collection of curves; at some points fiber tracts cross, kiss, branch, or merge [2, 4, 46]. Under those circumstances, two or three eigenvectors reflect fiber tract alignment. Second, noise and errors in the DT-MRI dataset may result in distorted eigenvalues and eigenvectors. In case two largest or all three eigenvectors differ by a small amount, the noise and errors may render the wrong dominant eigenvector [3, 7]. Based on the assumption, fiber tract extracting may fail to flow the true fiber tract trajectory.

To tackle the abovementioned problem, we use the anisotropy measures proposed by Westin et al. in [50], i.e. linearity, planarity, and sphericity, to classify the diffusion tensors into three types: linear, planar, and spherical. Given the linearity threshold, denoted by T_l where $0 \leq T_l \leq 1$,and the planarity threshold, denoted by T_p where $0 \leq T_p \leq 1$, we classify diffusion tensors into linear diffusion tensors, planar diffusion tensors, and spherical diffusion tensors using the following definitions: 1) a diffusion tensor is linear if its linearity exceeds the linearity threshold, i.e. $C_l > T_l$; 2) if a diffusion tensor is not linear, it is planar if its planarity exceeds the planarity threshold, i.e. $C_p > T_p$; and 3) if a diffusion tensor is neither linear or planar, it is spherical. The linearity threshold and planarity threshold are adjustable and should be appropriately assigned to faithfully reflect the nature of the human brain.

After the diffusion tensors are classified, for each diffusion tensor the eigenvector is selected and the weight of a certain edge is calculated by the following rules: 1) if the diffusion tensor is linear, select the dominant eigenvector and use it to calculate the weight of the edges; 2) if the diffusion tensor is planar, select two eigenvectors associated with two largest eigenvalues, use them to calculate the weight of the edge, resulting in two weight values, and assign the lower weight value to the edge; and 3) if the diffusion tensor is spherical, select all three eigenvectors, use them to calculate the weight of the edge, resulting in three weight values, and assign the lowest weight value to the edge.

2.5 Growing a DT-MRI minimum spanning tree

After all the edges have been assigned weight, use Prim's algorithm [40] to grow the minimum spanning tree.

2.6 Visualizing the DT-MRI minimum spanning tree

After the DT-MRI minimum spanning tree has been grown, visualize the edges of the tree using the average of fractional anisotropy, proposed by Basser and Pierpaoli in [9], of two adjacent vertices as a parameter of the opacity of the edge connecting the vertices.

3 Implementation and results

3.1 Implementation

The DT-MRI analysis, graph construction, and minimum spanning tree growing described in the previous section were implemented with in-house software written in C++. The DT-MRI data and minimum spanning tree visualization program was written using OpenGL and the Fast Light Toolkit (FLTK). The method was applied to a $256 \times 256 \times 53$ human brain DT-MRI dataset containing 548166 valid diffusion tensors. We constructed several graphs based on various combinations of linearity and planarity threshold values and in those graphs we grew minimum spanning trees by seeding them at voxels in several recognizable white matter structures.

3.2 Results

Figure 7 shows the minimum spanning tree seeded in the right internal capsule and comprised of 4000 nodes. The DT-MRI graph in which the minimum spanning tree was grown was constructed using the linearity threshold value of 0.15 and the planarity threshold value of 0.05. The minimum spanning tree represents the structure of the right internal capsule, the fiber bundle that connects the cerebral cortex and the subcortical structures. The minimum spanning tree displays the fanning and funneling of the sheet of fibers, which are consistent with the known anatomy of the internal capsule.

Figure 8 shows the minimum spanning tree seeded in the fiber bundle connecting the parietal lobe and the occipital lobe in the left cerebral hemisphere and comprised of 4500 nodes. The DT-MRI graph in which the minimum spanning tree was grown was constructed using the linearity threshold value of 0.15 and the planarity threshold value of 0.05. The minimum spanning tree represents the structure of the fiber bundle connecting the parietal lobe and the occipital lobe in the left cerebral hemisphere, successfully segregating the fiber bundle from the surrounding structures of the cerebrum. A part of the minimum spanning tree penetrates the cerebellum.

For comparison, Figure 9 shows the fiber tract trajectories computed from the same DT-MRI dataset using the technique explained in [8]. The fiber tracking stopped when fractional anisotropy became less than 0.35.

4 Conclusion

In this paper, we have presented a novel method for analyzing a DT-MRI dataset and visualizing the human brain using a minimum spanning tree. The minimum spanning tree has proven to be an effective tool for representing the human brain structure as it is a global deterministic model with well-defined connectivity. The minimum spanning tree acts as a connectivity map that shows the human brain fiber tract structures and facilitates global connectivity analysis.

Acknowledgments. First of all, I would like to thank Shigeo Takahashi for his kind supervision, valuable advice, and great patience. Next, I would like to express my gratitude to Chongke Bi for his expert guidance and extensive knowledge. I also appreciate courage and support from all members of Takahashi Laboratory. Finally, I would like to thank Jariya Pornpairat, Naphaporn Poolsin, Chanesd Srisukho, and all neurologists and physicians who have lent me their expertise in neuroanatomy and medical imaging.

References

1. Achard, S., Salvador, R., Whitcher, B., Suckling, J., Bullmore, E.: A resilient, low-frequency, small-world human brain functional network with highly connected association cortical hubs. The Journal of Neuroscience 26(1), 63–72 (2006)
2. Basser, P.J.: New histological and physiological stains derived from diffusion-tensor mr images. Annals of the New York Academy of Sciences 820(1), 123–138 (1997)
3. Basser, P.J.: Quantifying errors in fiber tract direction and diffusion tensor field maps resulting from mr noise. In: Proceedings of the 5th Annual Meeting of ISMRM, Vancouver, Canada. p. 1740 (1997)
4. Basser, P.J.: Fiber-tractography via diffusion tensor MRI (DT-MRI). In: Proceedings of the 6th Annual Meeting ISMRM, Sydney, Australia. vol. 1226 (1998)
5. Basser, P.J., Mattiello, J., LeBihan, D.: Estimation of the effective self-diffusion tensor from the nmr spin echo. Journal of Magnetic Resonance, Series B 103(3), 247–254 (1994)
6. Basser, P.J., Mattiello, J., LeBihan, D.: Mr diffusion tensor spectroscopy and imaging. Biophysical journal 66(1), 259–267 (1994)
7. Basser, P.J., Pajevic, S.: Statistical artifacts in diffusion tensor MRI (DT-MRI) caused by background noise. Magnetic Resonance in Medicine 44(1), 41–50 (2000)
8. Basser, P.J., Pajevic, S., Pierpaoli, C., Duda, J., Aldroubi, A.: In vivo fiber tractography using DT-MRI data. Magnetic resonance in medicine 44(4), 625–632 (2000)

9. Basser, P.J., Pierpaoli, C.: Microstructural and physiological features of tissues elucidated by quantitative-diffusion-tensor MRI. Journal of Magnetic Resonance, Series B 111(3), 209–219 (1996)
10. Behrens, T., Johansen-Berg, H., Woolrich, M., Smith, S., Wheeler-Kingshott, C., Boulby, P., Barker, G., Sillery, E., Sheehan, K., Ciccarelli, O., et al.: Non-invasive mapping of connections between human thalamus and cortex using diffusion imaging. Nature neuroscience 6(7), 750–757 (2003)
11. Buckner, R.L., Andrews-Hanna, J.R., Schacter, D.L.: The brain's default network. Annals of the New York Academy of Sciences 1124(1), 1–38 (2008)
12. Ramón y Cajal, S.: Histology of the nervous system of man and vertebrates. Oxford Univ. Press, New York (1995)
13. Conturo, T.E., Lori, N.F., Cull, T.S., Akbudak, E., Snyder, A.Z., Shimony, J.S., McKinstry, R.C., Burton, H., Raichle, M.E.: Tracking neuronal fiber pathways in the living human brain. Proceedings of the National Academy of Sciences 96(18), 10422–10427 (1999)
14. Ge, Y., Law, M., Grossman, R.I.: Applications of diffusion tensor mr imaging in multiple sclerosis. Annals of the New York Academy of Sciences 1064(1), 202–219 (2005)
15. Hagmann, P., Cammoun, L., Gigandet, X., Meuli, R., Honey, C.J., Wedeen, V.J., Sporns, O.: Mapping the structural core of human cerebral cortex. PLoS biology 6(7), e159 (2008)
16. Haier, R.J., Jung, R.E., Yeo, R.A., Head, K., Alkire, M.T.: Structural brain variation and general intelligence. NeuroImage 23(1), 425–433 (2004)
17. Haier, R.J., Jung, R.E., Yeo, R.A., Head, K., Alkire, M.T.: The neuroanatomy of general intelligence: sex matters. NeuroImage 25(1), 320–327 (2005)
18. van den Heuvel, M., Mandl, R., Luigjes, J., Pol, H.H.: Microstructural organization of the cingulum tract and the level of default mode functional connectivity. The Journal of neuroscience 28(43), 10844–10851 (2008)
19. Hlawitschka, M., Scheuermann, G., Hamann, B.: Interactive glyph placement for tensor fields. In: Advances in Visual Computing, pp. 331–340. Springer (2007)
20. Honey, C., Sporns, O., Cammoun, L., Gigandet, X., Thiran, J.P., Meuli, R., Hagmann, P.: Predicting human resting-state functional connectivity from structural connectivity. Proceedings of the National Academy of Sciences 106(6), 2035–2040 (2009)
21. Jones, D.K.: Diffusion MRI: Theory, methods, and applications. Oxford University Press (2010)
22. Jones, D.K., Simmons, A., Williams, S.C., Horsfield, M.A.: Non-invasive assessment of axonal fiber connectivity in the human brain via diffusion tensor MRI. Magnetic Resonance in Medicine 42(1), 37–41 (1999)
23. Kindlmann, G., Weinstein, D.: Hue-balls and lit-tensors for direct volume rendering of diffusion tensor fields. In: Proceedings of the conference on Visualization'99: celebrating ten years. pp. 183–189. IEEE Computer Society Press (1999)
24. Kindlmann, G., Westin, C.F.: Diffusion tensor visualization with glyph packing. Visualization and Computer Graphics, IEEE Transactions on 12(5), 1329–1336 (2006)
25. Koch, M.A., Norris, D.G., Hund-Georgiadis, M.: An investigation of functional and anatomical connectivity using magnetic resonance imaging. Neuroimage 16(1), 241–250 (2002)
26. Kruggel, F.: MRI-based volumetry of head compartments: normative values of healthy adults. Neuroimage 30(1), 1–11 (2006)
27. Le Bihan, D., Mangin, J.F., Poupon, C., Clark, C.A., Pappata, S., Molko, N., Chabriat, H.: Diffusion tensor imaging: concepts and applications. Journal of magnetic resonance imaging 13(4), 534–546 (2001)
28. Li, Y., Liu, Y., Li, J., Qin, W., Li, K., Yu, C., Jiang, T.: Brain anatomical network and intelligence. PLoS computational biology 5(5), e1000395 (2009)
29. Marner, L., Nyengaard, J.R., Tang, Y., Pakkenberg, B.: Marked loss of myelinated nerve fibers in the human brain with age. Journal of Comparative Neurology 462(2), 144–152 (2003)
30. Mori, S., Crain, B.J., Chacko, V., Van Zijl, P.: Three-dimensional tracking of axonal projections in the brain by magnetic resonance imaging. Annals of neurology 45(2), 265–269 (1999)

31. Mori, S., van Zijl, P.: Fiber tracking: principles and strategies–a technical review. NMR in Biomedicine 15(7-8), 468–480 (2002)
32. Mukherjee, P.: Diffusion tensor imaging and fiber tractography in acute stroke. Neuroimaging Clinics of North America 15(3), 655–665 (2005)
33. Nolte, J.: The human brain: An introduction to its functional anatomy, st. louis: Mosby (2002)
34. Oldendorf, W.: The quest for an image of brain: a brief historical and technical review of brain imaging techniques. Neurology 28(6), 517–533 (1978)
35. Parker, G.J., Alexander, D.C.: Probabilistic monte carlo based mapping of cerebral connections utilising whole-brain crossing fibre information. In: Information Processing in Medical Imaging. pp. 684–695. Springer (2003)
36. Parker, G.J., Alexander, D.C.: Probabilistic anatomical connectivity derived from the microscopic persistent angular structure of cerebral tissue. Philosophical Transactions of the Royal Society B: Biological Sciences 360(1457), 893–902 (2005)
37. Peled, S., Gudbjartsson, H., Westin, C.F., Kikinis, R., Jolesz, F.A.: Magnetic resonance imaging shows orientation and asymmetry of white matter fiber tracts. Brain research 780(1), 27–33 (1998)
38. Pierpaoli, C., Jezzard, P., Basser, P.J., Barnett, A., Di Chiro, G.: Diffusion tensor mr imaging of the human brain. Radiology 201(3), 637–648 (1996)
39. Poupon, C., Clark, C., Frouin, V., Regis, J., Bloch, I., Le Bihan, D., Mangin, J.F.: Regularization of diffusion-based direction maps for the tracking of brain white matter fascicles. Neuroimage 12(2), 184–195 (2000)
40. Prim, R.C.: Shortest connection networks and some generalizations. Bell system technical journal 36(6), 1389–1401 (1957)
41. Sporns, O., Chialvo, D.R., Kaiser, M., Hilgetag, C.C.: Organization, development and function of complex brain networks. Trends in cognitive sciences 8(9), 418–425 (2004)
42. Stam, C.J., Reijneveld, J.C.: Graph theoretical analysis of complex networks in the brain. Nonlinear biomedical physics 1(1), 3 (2007)
43. Swanson, L.W.: Brain architecture: understanding the basic plan. Oxford University Press (2012)
44. Tang, Y., Nyengaard, J.R.: A stereological method for estimating the total length and size of myelin fibers in human brain white matter. Journal of neuroscience methods 73(2), 193–200 (1997)
45. Tench, C., Morgan, P., Blumhardt, L., Constantinescu, C.: Improved white matter fiber tracking using stochastic labeling. Magnetic resonance in medicine 48(4), 677–683 (2002)
46. Tournier, J., Calamante, F., Connelly, A., et al.: Mrtrix: diffusion tractography in crossing fiber regions. International Journal of Imaging Systems and Technology 22(1), 53–66 (2012)
47. Werring, D.J., Toosy, A.T., Clark, C.A., Parker, G.J., Barker, G.J., Miller, D.H., Thompson, A.J.: Diffusion tensor imaging can detect and quantify corticospinal tract degeneration after stroke. Journal of Neurology, Neurosurgery & Psychiatry 69(2), 269–272 (2000)
48. Werring, D., Clark, C., Barker, G., Miller, D., Parker, G., Brammer, M., Bullmore, E., Giampietro, V., Thompson, A.: The structural and functional mechanisms of motor recovery: complementary use of diffusion tensor and functional magnetic resonance imaging in a traumatic injury of the internal capsule. Journal of Neurology, Neurosurgery & Psychiatry 65(6), 863–869 (1998)
49. Werring, D., Clark, C., Barker, G., Thompson, A., Miller, D.: Diffusion tensor imaging of lesions and normal-appearing white matter in multiple sclerosis. Neurology 52(8), 1626–1626 (1999)
50. Westin, C.F., Peled, S., Gudbjartsson, H., Kikinis, R., Jolesz, F.A., et al.: Geometrical diffusion measures for MRI from tensor basis analysis. In: Proceedings of ISMRM. vol. 97, p. 1742 (1997)
51. Witwer, B.P., Moftakhar, R., Hasan, K.M., Deshmukh, P., Haughton, V., Field, A., Arfanakis, K., Noyes, J., Moritz, C.H., Meyerand, M.E., et al.: Diffusion-tensor imaging of white matter tracts in patients with cerebral neoplasm. Journal of neurosurgery 97(3), 568–575 (2002)

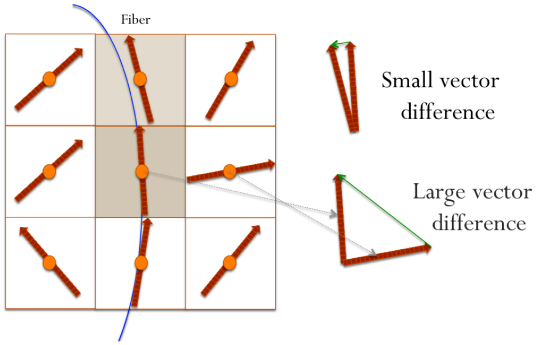

Fig. 1.

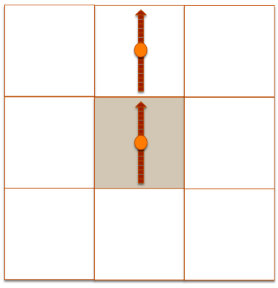

Fig. 2.

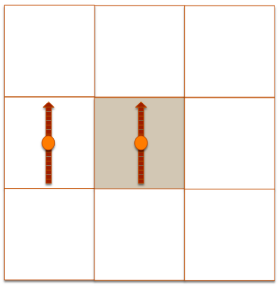

Fig. 3.

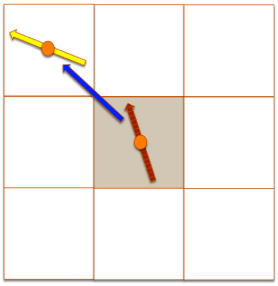

Fig. 4.

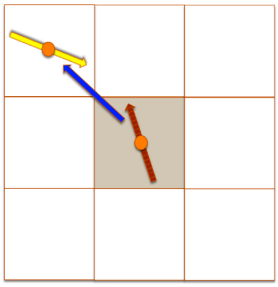

Fig. 5.

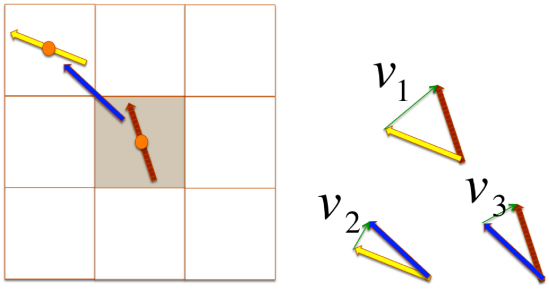

Fig. 6.

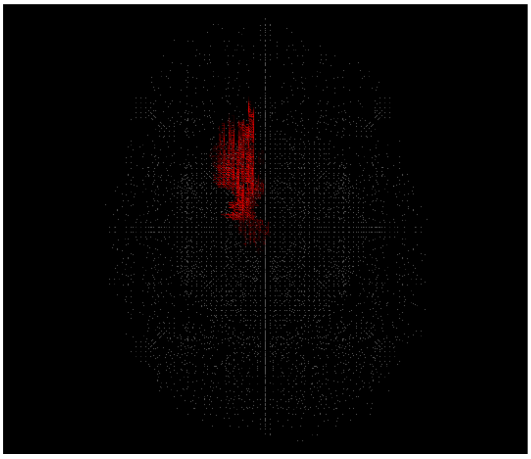

Fig. 7.

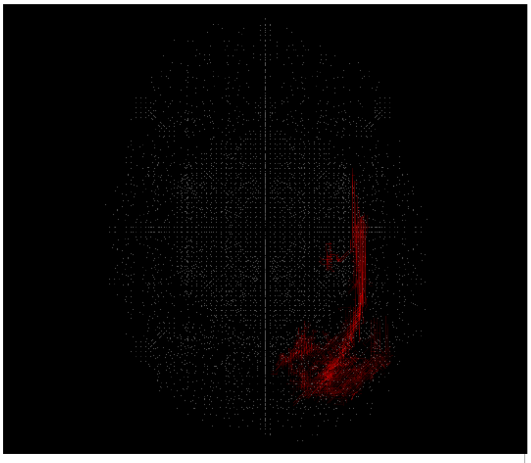

Fig. 8.

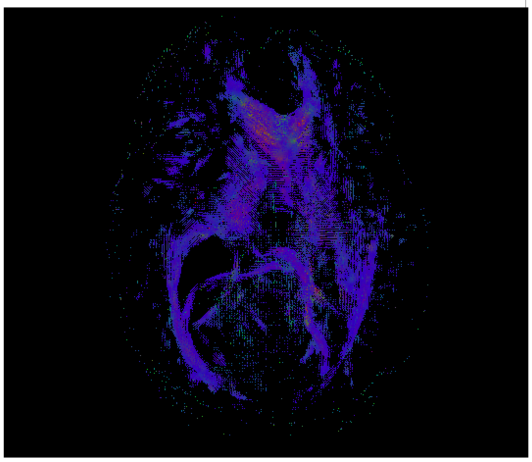

Fig. 9.